Whole-Brain Imaging with Receive-only Multichannel Top-hat Dipole Antenna RF Coil at 7T MRI

Suchit KUMAR

Department of Biomicrosystem Technology, Korea University, Seoul 02842, Korea

Jun-Sik YOON, Jong-Min KIM

Department of Electronics and Information Engineering, Korea University, Sejong 30019, Korea

Chulhyun LEE

Bioimaging Research Team, Korea Basic Science Institute, Ochang 28119, Korea

Chang-Hyun OH*

Department of Electronics and Information Engineering, Korea University, Sejong 30019, Korea

This work investigates the construction and performance of an eight-channel top-hat dipole receiver RF coil with a capacitive plate to increase the longitudinal whole-brain coverage and receiver sensitivity gain in the brain at 7T MRI. The construction method for top-hat dipole-based receiver RF coil by adjusting the length and structure corresponding to each channel consists of tuning, matching, balun, and detuning circuitry. Electromagnetic simulations were analyzed on a 3-D human model to evaluate B_1^+ efficiency and specific absorption rate deposition. Coil performance was evaluated in the human head imaging in vivo. EM simulation results indicated a higher B_1^- sensitivity in the brain and z-directional coverage of the proposed eight-channel receiver RF coil. The MR images were acquired with an identical field of view showing the receiver coverage improvement in the brain when capacitive plates are used. The MR images also show the clear visibility of the complete set of the cervical vertebrae as well as

the spinal cord. The acquired MRI results demonstrate the capability of the proposed RF coil to increase the receiver coverage in the longitudinal direction. Moreover, the B_1^+ efficiency, as well as receiver sensitivity in the brain, can be substantially improved with the use of multilayered capacitive plates of proper shape and size in conjunction with an RF coil.

PACS number:

Keywords: Magnetic resonance imaging (MRI), top-hat dipole antenna, receive RF coil, 7T MRI, whole-brain imaging, EM modeling & simulation

Email: ohch000@gmail.com

Fax: +82-2-3290-3984

I. INTRODUCTION

Ultrahigh-field-magnetic resonance imaging (UHF-MRI ≥7T) has several advantages including higher resolution in both anatomical and functional imaging; higher signal-to-noise (SNR) ratio; and higher T1, T2, and T2* (susceptibility) tissue contrasts. Due to these advantages, UHF-MRI is the most versatile choice to image both anatomical and functional changes in the brain [1,2]. Radiofrequency (RF) coils are an essential part of the MRI system, and many designs have been reported to improve both transmission and reception at 7T MRI [3-8]. In general, quadrature birdcage RF coil for transmission and multichannel surface loop RF coil for the reception are widely preferred. In addition, the transceiver birdcage RF coil during reception shows a higher signal at the center than at the periphery (also known as central brightening) and the receive surface RF coil shows high SNR near the periphery [9]. The major problems associated with the surface loop coil designs are the smaller field of view (FOV) and lower sensitivity in the deep region of the target. The close fit and denser receiver coil arrays have been previously implemented to increase the FOV and receiver coil sensitivity [10]. The approach to increase the FOV and SNR were usually focused on either increasing the dimensions of the loop RF coil or the number of receiver channels. However, no significant improvements were noted by increasing the number of channels in the RF coil designs other than the peripheral SNR [11]. Moreover, increasing the number of channels in the receiver loop RF coil raises the difficulty in decoupling between neighboring channels.

Furthermore, the ultimate intrinsic SNR (UISNR) approach understands the achievable SNR contribution of the receiver coil at different field strengths [12,13]. These studies pointed out that two types of surface current distribution, e.g., divergence- and curl-free currents, could contribute to optimum SNR when combined. Moreover, the surface loop coil contributes to the divergence-free current pattern only, whereas the radiative antenna such as the z-directed dipole antenna contributes to the combination of curl- and divergence-free current patterns. Various radiative antennas (e.g., dipole

and monopole) have already been investigated and reported for brain imaging [14-16]. These studies suggested that the antenna can increase the B_1 field penetration in the target at a deep location as well as transmit efficiency compared to other RF coil designs at higher field strength. The dipole antenna has higher and symmetric B_1 field distribution than the surface loop coil which makes it an excellent choice for RF coil at UHF. Another report mentioned that the use of monopole antenna for brain imaging can improve both transmission efficiency and receiver sensitivity [14]. Moreover, a report exists on dipole antenna-based receiver coil design using a 29-channel short dipole antenna RF coil array at 7T MRI [17], showing high performance for whole-brain imaging but suffers from the mutual coupling between neighboring channels.

In addition, the commercially available human head RF coil at 7T MRI is primarily focused in the upper region (e.g., cerebrum, corpus collosum, and cerebellum) of the head and provides less sensitivity at the cervical spinal cord (C-spine). Commercial head RF coil has a deteriorated performance in neuroimaging studies with C-spine disorders, and a dedicated RF coil is required for C-spine imaging [18]. Furthermore, another paper reported that the eight-channel transmit and 15-channel receive head neck RF coil is designed for whole-brain MRI [19]. However, the eight-channel parallel transmission is yet to receive the Food and Drug Administration approval for clinical daily routine examinations. Thus, this study focuses on multichannel receive-only RF coil insert with commercial transmit RF coil for whole-brain MRI imaging to keep the clinical constraint.

This study implemented the top-hat dipole antenna which is a modified dipole antenna for brain reception [20]. The top-hat dipole antenna is a combination of the conventional dipole antenna and a top-hat conductor (e.g., metal disk, radial wires, and metal sphere) attached at each ends of the dipole arms. Adding the top-hat conductor to the ends of the dipole antenna increases the transmission and reception efficiency. This is achieved mainly by the addition of a large piece of metal at the top of the dipole arms which leads to an increase in the capacitance from the top of the antenna to the reference plane and an increase in the current flow to the top of the antenna. In addition, a capacitive plate

positioned above the RF coil and imaging object was considered to increase the sensitivity in the upper region. Kang et al. [21] utilized a similar approach with a simple copper plate. However, implementing their approach in this work shows severe artifacts in the MR images. Thus, to solve this problem, a capacitive plate was designed, consisting of multilayered sheets of the copper patch with a very small gap between the sheets, sandwiched with a dielectric to generate capacitance, and tightly fixed on the RF coil frame to sustain less vibration.

This study aims to increase longitudinal FOV coverage and overall receiver sensitivity for whole-brain imaging at 7T MRI. Moreover, the top-hat dipole antenna-based eight-channel receiver RF coil for the human head was constructed and evaluated in this work through electromagnetic (EM) simulations and *in vivo* MRI experiments.

II. MATERIALS AND METHODS

1. EM Simulations

EM modeling and simulations are extensively utilized in the MRI to optimize the RF coil performance in terms of design, EM fields, and safety before RF coil manufacturing [22,23]. EM simulations based on finite difference time domain (FDTD) were conducted using a commercial FDTD simulator (SIM4LIFE, ZMT, Zurich, Switzerland) on a 3D human model Duke (305 parametric tissues) [24]. First, one-channel RF coil simulations were performed to visualize and analyze the B_1 field distribution for surface loop, dipole, and top-hat dipole antenna RF coil (refer to supplementary file). Second, a combination of a two-port transmit RF coil and an eight-channel receiver RF coil were simulated to analyze the effect of the receiver RF coil on the B_1^+ field as well as the specific absorption rate (SAR) distribution of transmitting RF coil and their respective B_1^- field.

For transmission, a high-pass birdcage RF coil was simulated and driven with two ports having the same amplitude and 90°-phase difference between each port as shown in Fig. 1a. The quadrature birdcage coil used in this simulation is a generic head RF coil which consists of 12 legs (width, 1 cm;

length, 20 cm; radius, 15 cm) and an RF shield (length, 30 cm; radius, 18.75 cm). Moreover, the capacitive plate has negligible effect on the end-ring capacitor and impedance of the birdcage coil.

For the reception, the top-hat dipole RF coil without/with a capacitive plate was simulated as shown in Fig. 1b, c, respectively. A T-network circuit consisting of two inductors and a capacitor was used to tune and match the top-hat dipole. The capacitive plate of the multilayered sheets was made using square patches of copper and capacitance was generated between each layer by inserting dielectric material (relative permittivity, 2.3; identical to the polyimide material). The equivalent impedance of the capacitive plate is much lower than 50 ohms at 298 MHz and operate almost like a short circuit. On the contrary, in relation to the gradient fields which are commonly switched at low frequencies in the kHz range, the impedance of the capacitive plate is very high and almost invisible to the gradient field. The plate was placed 1 cm above the RF coil in both the EM simulation and MRI experiments.

After performing the EM simulation, the signal intensity (SI) distribution for gradient-echo (GE) can be estimated from the transmit (B_1^+) and receive (B_1^-) field neglecting the T_2 decay as the following equation [25]:

$$SI \propto |conj(B_1^-)|sin(|B_1^+|\gamma\tau) \quad (1)$$

where *SI* is the simulated GRE image, B_1^+ is the transmit B_1 field from the transmit (birdcage) RF coil (normalized to 1.957 μT at the center of the coil), $conj(B_1^-)$ is the conjugate of the receive B_1 field from the receiver (top-hat) RF coil, γ is the gyromagnetic ratio (42.576 MHz/T), and τ is the RF pulse duration (assuming 3 ms, 90° flip angle [FA]).

2. Coil Design and Benchmark Tests

The schematics of the one-channel and constructed eight-channel top-hat dipole RF coil without/with capacitive plate configuration are shown in Fig. 2. The coil length was tuned to 25 cm for sufficient coverage of the human head by using a T-network tuning/matching circuit. Detuning circuits using pin

diodes (MA4P4002B-402, MACOM, Lowell, MA, USA) were implemented in the coil circuit to detune the receiver coils during RF transmission. The multilayered capacitive plate was constructed using copper patches in a circular shape as shown in Fig. 2d. The reflection coefficient (S_{11}) for the eight-channel and decoupling coefficient (S_{21}) between neighboring channels were measured using a vector network analyzer (N9913A, Agilent Technologies, Carpinteria, CA, USA). Figure 2 shows that the constructed left-side RF coil (Fig. 2c) utilizes the coaxial-type balun consists of two coaxial cables of $\lambda/4$ and $3\lambda/4$ length and the right-side constructed RF coil (Fig. 2d) utilizes the lattice LC-type balun consists of two inductors and two capacitors connected as lattice, which is more stable in impedance measurement and very compact in design than coaxial-type balun.

3. MRI Experiments

All images were acquired using Achieva 7T MRI (Philips Healthcare, Best, The Netherlands). A commercial head birdcage RF coil (Nova Medical, Inc., Wilmington, MA, USA) was used for transmission and proposed eight-channel top-hat dipoles with/without capacitive plate were used for reception. *In vivo* brain MRI experiments were performed on healthy volunteers as following: (I) Flip angle (FA or B_1) mapping using dual TR gradient echo (GE) sequence [26], (II) High resolution MR images of brain using 3D T1-weighted magnetization-prepared rapid gradient-echo (3D T1w-MPRAGE) sequence, and (III) T2*-weighted multiple fast field echo (T2*w-mFFE) sequence, the scan parameters are shown in Table 1.

Our Institutional Review Board approved the study and written informed consent was obtained from all the volunteers before the start of the experiments (approval number is mentioned in the acknowledgement).

III. RESULTS

1. EM Simulations

Through the EM simulation, it was found that the dipole antenna has more symmetric B_1 field distribution than the surface loop RF coil (refer to the supplementary file). The B_1^+ field distribution of the birdcage RF coil was obtained with quadrature feeding. Subsequently, the B_1^- field distribution for the eight-channel top-hat dipole RF coil was obtained, and simulated SI distribution were generated using Eq. (1) in MATLAB. The simulated B_1^+ field from the birdcage (TX) only, birdcage (TX)/top-hat dipole (RX) without capacitive plate, and birdcage (TX)/top-hat dipole (RX) with capacitive plate are shown in Fig. 3a–c. The magnitude of B_1^+ field was increased by 5.5% at the center and 41.41% at the upper part of the head when the capacitive plate was used. The simulated SI distribution from the birdcage RF coil, eight-channel top-hat dipole RF coil without capacitive plate, and eight-channel top-hat dipole RF coil with capacitive plate are shown in Fig. 3d–f. The result shows increased sensitivity in the brain for the eight-channel top-hat dipole RF coil with capacitive plate. Furthermore, the 10g-avg SAR distribution for the birdcage (TX) only, birdcage (TX)/top-hat dipole (RX) without capacitive plate, and birdcage (TX)/top-hat dipole (RX) with capacitive plate were 0.1342W/kg (avg), 0.489 W/kg (max); 0.1385 W/kg (avg), 0.4724 W/kg (max); and 0.132 W/kg (avg), 0.576 W/kg (max), respectively. The total input powers do not change much (<10% variation) for the birdcage without/with RX coil, and the peak 10 g-avg SAR values in all the RF coils are under the IEC SAR limits (refer to IEC's 60601-2-33).

2. MRI Experiments

S-parameter and quality factor analysis were performed for the eight-channel top-hat dipole RF coil to ensure proper tuning, matching, and decoupling of each channel. Coil elements were tuned and matched to 50-Ω with measured reflection coefficient (S_{11}) for the eight channels were −30 dB or less at 298 MHz, and the decoupling coefficient (S_{21}) between neighboring channels were −15 dB or less.

The ratio of unloaded to loaded Q (QU/QL) for the top-hat dipole antenna without/with capacitive plate were approximately 4.6 and 4.9, respectively, which is considered acceptable for RF coil analysis indicating the dominance of noise from the target. Figure 4a, b shows the FA maps of the brain acquired at the sagittal plane using the eight-channel top-hat dipole RF coil without/with capacitive plate, which clearly shows the B_1^+ field enhancement using the capacitive plate. The 3D T1w-MPRAGE and T2w-mFFE MR images at the sagittal plane using the eight-channel top-hat dipole RF coil without and with capacitive plate are shown in Fig. 4c-f. Low SI was observed on the upper region of the brain using the eight-channel top-hat dipole RF coil without the capacitive plate and the eight-channel top-hat dipole RF coil with capacitive plate clearly shows the sensitivity gain at the upper region as well as clear visibility of the cervical vertebrae at the C-2 to C-7 level and spinal cord as shown in Fig. 4c, d. Figure 4e, f shows the T2*w contrast in the brain and spinal cord at different TE interval.

IV. DISCUSSION AND CONCLUSION

This work evaluated the receiver performance of the eight-channel top-hat dipole RF coil with a capacitive plate. The proposed receiver RF coil exhibits lower coupling with the transmit RF coil and does not deteriorate the B_1^+ field. In addition, the RF coil with a capacitive plate also improves both B_1^+ field distribution as well as receiver sensitivity in the brain and was able to cover the entire portion of the head including the cervical vertebrae.

In the first design, the top-hat dipoles were placed on the helmet-shaped 3D-printed RF coil frame without a capacitive plate. However, no special reason exists for using a 3D-printed RF coil frame other than the proximity of the RF coil to the imaging target. In this initial design, coaxial-type balun was used for the source feeding, but it suffered from very high sensitivity in impedance measurement rising from a very small movement in the coaxial cable which suggested in the consideration of lumped element-based lattice LC-type balun. The MRI images acquired using this design exhibited less signal

sensitivity in the upper region of the head. However, the C-spine was covered. This led to the consideration of alternatives for the enhancement of signals in the upper region of the head.

In the second design, the RF coil frame was made using an acrylic cylindrical hollow structure to facilitate the proper positioning of the capacitive plate above the RF coil (Fig. 2d). This design included the lattice LC-type balun for the source feeding. The MRI images show higher signal sensitivity in the upper region of the head compared with the first design as well as higher signal coverage in the C-spine region. Alternatively, the top-hat dipole RF coil can be constructed on the helmet-shaped RF coil frame, and the capacitive plate can be modified to the skullcap structure to further increase the filling factor between the RF coil and the imaging target, which could further improve receiver sensitivity as well as the SNR.

Moreover, this work only used a single-row configuration (1 × 8) of the eight-channel top-hat dipole RF coil to cover the whole brain. Therefore, implementing the high-density of 16- (2 × 8) or 32-channel (2 × 16 or 4 × 8) shortened top-hat dipole RF coil could be beneficial to further improve the SNR and acceleration to decrease the acquisition scan times. Furthermore, in terms of transmission RF coil design, the eight-channel top-hat dipole RF coil showed promising results in EM simulation analysis to achieve better transmission efficiency and reduced SAR [27,28]. Therefore, the proposed RF coil can be used for the multichannel or parallel transmission RF coil design at UHF-MRI with proper detuning and a T/R switching mechanism.

In conclusion, the proposed eight-channel top-hat dipole RF coil improves the longitudinal coverage and the transmission as well as the receiver sensitivity of the whole-brain imaging at 7T MRI.

ACKNOWLEDGEMENT

This work was supported by the Korea Medical Device Development Fund (Project Number: 1711138003, KMDF-RnD KMDF_PR_20200901_0041-2021-02) grant funded by the Korea government (the Ministry of Science and ICT, the Ministry of Trade, Industry and Energy, the Ministry of Health & Welfare, the Ministry of Food and Drug Safety). ZMT is appreciated for providing the free license of Sim4Life used in this study. The study was conducted and approved by the Institutional Review Board of KOREA UNIVERSITY (KUIRB-2021-0143-01, date of approval–2021-05-11).

REFERENCES

[1] A. G. V. D. Kolk, J. Hendrikse, J. J. Zwanenburg, F. Visser, and P. R. Luijten, Eur J Radiol. **82(5)**, 708 (2013). https://doi.org/10.1016/j.ejrad.2011.07.007.

[2] M. Metcalf et al., J Neuroimaging. **20(2)**, 141 (2010). https://doi.org/10.1111/j.1552-6569.2008.00338.x.

[3] J. T. Vaughan et al., Magn Reson Med. **47(5)**, 990 (2002). https://doi.org/10.1002/mrm.10141.

[4] J. Hoffmann, G. Shajan, J. Budde, K. Scheffler, and R. Pohmann, Magn Reson Med. **69(5)**, 1494 (2013). https://doi.org/10.1002/mrm.24367.

[5] N. I. Avdievich, S. Oh, H. P. Hetherington, and C. M. Collins, J Magn Reson Imaging. **32(2)**, 476 (2010). https://doi.org/10.1002/jmri.22257.

[6] C. Wang, G. X. Shen, J Magn Reson Imaging. **24(2)**, 439 (2006). https://doi.org/10.1002/jmri.20635.

[7] G. Adriany et al., Magn Reson Med. **59(3)**, 590 (2008). https://doi.org/10.1002/mrm.21488.

[8] N. I. Avdievich, J. W. Pan, J. M. Baehring, D. D. Spencer, and H. P. Hetherington, Magn Reson Med. **62(1)** ,17 (2009). https://doi.org/10.1002/mrm.21970.

[9] G. C. Wiggins et al., Magn Reson Med. **56(1)**, 216 (2006). https://doi.org/10.1002/mrm.20925.

[10] G. C. Wiggins et al., Magn Reson Med. **62(3)**, 754 (2009). https://doi.org/10.1002/mrm.22028.

[11] D. K. Spence, S. M. Wright, Concepts Magn Reson. B. **31(2)**, 86 (2007). https://doi.org/10.1002/cmr.b.20088.

[12] B. Guerin et al., Magn Reson Med. **78(5)**, 1969 (2017). https://doi.org/10.1002/mrm.26564.

[13] R. Lattanzi et al., Magn Reson Med. **79(3)**, 1789 (2018). https://doi.org/10.1002/mrm.26803.

[14] S. M. Hong, J. H. Park, M. K. Woo, Y. B. Kim, and Z. H. Cho, Magn Reson Med. **71(5)**, 1944 (2014). https://doi.org/10.1002/mrm.24844.

[15] J. D. Clément, R. Gruetter, and Ö. Ipek, Magn Reson Med. **81(2)**, 1447 (2019). https://doi.org/10.1002/mrm.27476.

[16] N. I. Avdievich, G. Solomakha, L. Ruhm, Scheffler K, and A. Henning, Magn Reson Med. **82(2)**, 811 (2019). https://doi.org/10.1002/mrm.27754.

[17] B. Zhang et al., in Proceedings of the 25th Annual Meeting of ISMRM, Honolulu, HI, pp. 4314 (2017).

[18] B. Zhang, A. C. Seifert, J. W. Kim, J. Borrello, and J. Xu, Magn Reson Med. **78(4)**, 1623 (2017). https://doi.org/10.1002/mrm.26538.

[19] V. Pfaffenrot et al., Magn Reson Med. **80(3)**, 1252 (2018). https://doi.org/10.1002/mrm.27125.

[20] C. H. Oh et al, in Proceedings of the 25th Annual Meeting of ISMRM, Honolulu, HI, pp. 0767 (2017).

[21] C. K. Kang et al., Magn Reson Med. **60(2)**, 330 (2008). https://doi.org/10.1002/mrm.21472.

[22] V. Chen, M. Steckner, Med. Phys. **44(3)**, 1186 (2017). https://doi.org/10.1002/mp.12103.

[23] N. Krishnamurthy, T. Zhao, T. S. Ibrahim, J Magn Reson Imaging. **39(2)**, 475 (2014). https://doi.org/10.1002/jmri.24152.

[24] M. Gosselin, E. Neufeld, H. Moser, Phys Med Biol. **59(18)**, 5287 (2014). https://doi.org/10.1088/0031-9155/59/18/5287.

[25] C. M. Collins, M. B. Smith, Magn Reson Med. **45(4)**, 684 (2001). https://doi.org/10.1002/mrm.1091.

[26] V. L. Yarnykh, Magn Reson Med. **57(1)**, 192 (2007). https://doi.org/10.1002/mrm.21120.

[27] S. Kumar et al., in Proceedings of the 24th Annual Meeting of ISMRM, Singapore, pp. 2149 (2016).

[28] S. Kumar et al., in Proceedings of the 25th Annual Meeting of ISMRM, Honolulu, HI, pp. 2659 (2017).

Fig. 1.

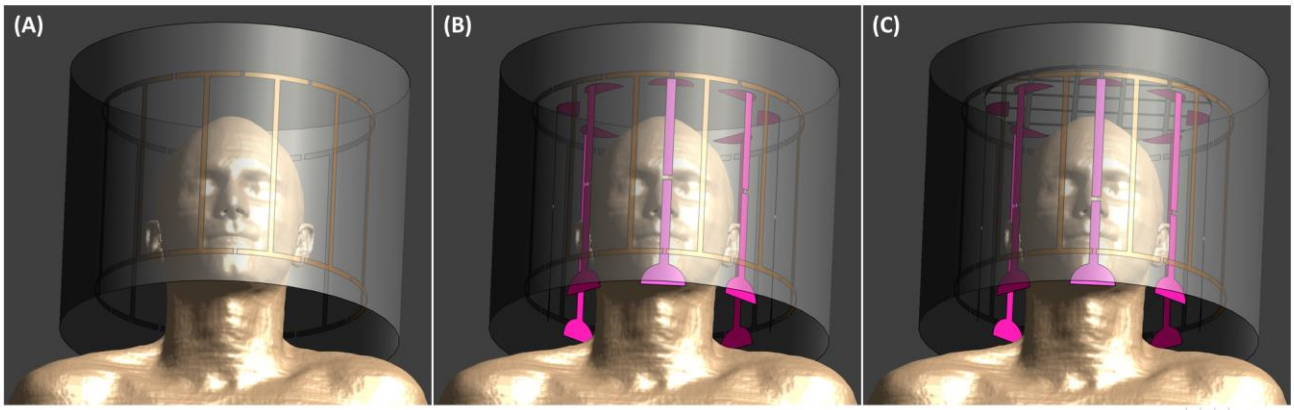

12 leg high-pass birdcage
- RF coil diameter – 150 mm
- RF coil length – 200 mm
- RF shield diameter – 187.5 mm
- RF shield length – 300 mm

*Dimensions are identical to commercial birdcage

8-channel top-hat dipole RF coil
- Top-hat half-disc – 25 mm
- RF coil length – 250 mm
- Source position – center

8-channel top-hat dipole RF coil
- Top-hat half-disc – 25 mm
- RF coil length – 250 mm
- Source position – 1.5:1

Capacitive plate – 3 layered with dielectric material in between
- Diameter – 125 mm

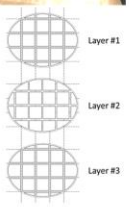

Fig. 2.

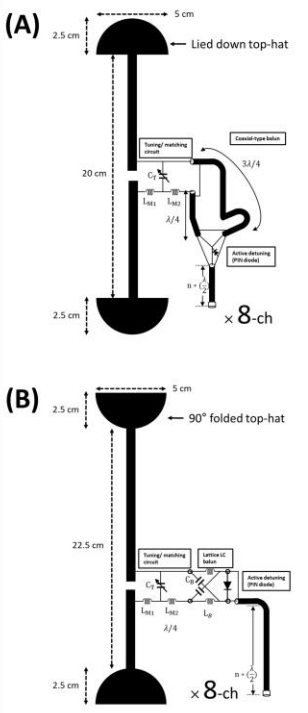

*RF coil frame was constructed using 3D printer.
*Coaxial-type balun was used.

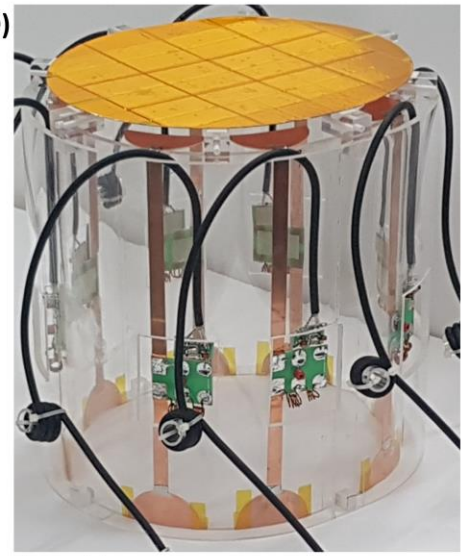

*RF coil frame was constructed using acrylic material.
*Lattice LC-type balun was used.

Fig. 3.

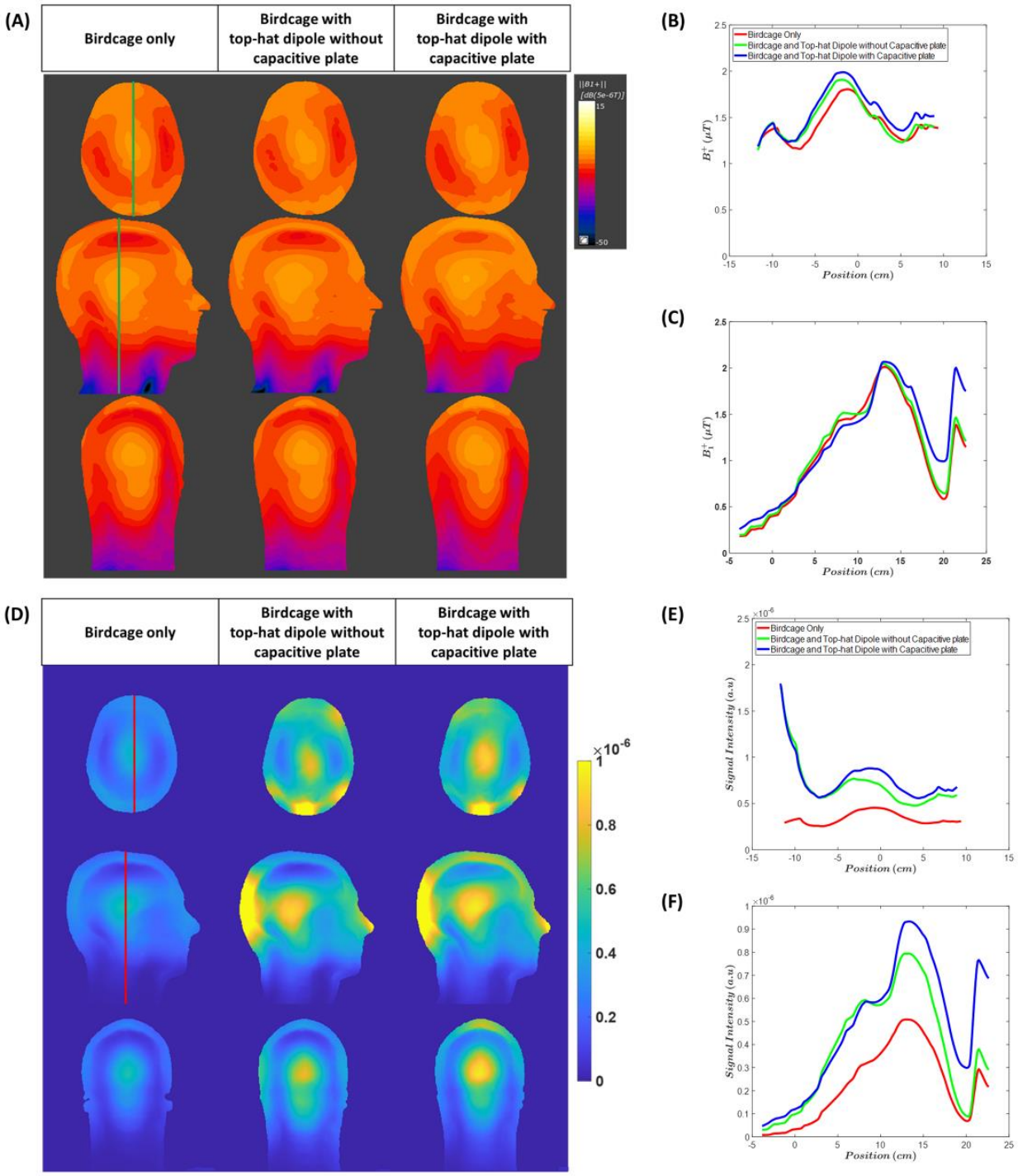
(A)
Birdcage only
Birdcage with top-hat dipole without capacitive plate
Birdcage with top-hat dipole with capacitive plate
||B1+||
[dB(5e-6T)]
15
-50
(B)
Birdcage Only
Birdcage and Top-hat Dipole without Capacitive plate
Birdcage and Top-hat Dipole with Capacitive plate
B_1^+ (μT)
Position (cm)
(C)
B_1^+ (μT)
Position (cm)
(D)
Birdcage only
Birdcage with top-hat dipole without capacitive plate
Birdcage with top-hat dipole with capacitive plate
×10-6
(E)
Birdcage Only
Birdcage and Top-hat Dipole without Capacitive plate
Birdcage and Top-hat Dipole with Capacitive plate
Signal Intensity (a.u)
Position (cm)
(F)
Signal Intensity (a.u)
Position (cm)

Fig. 4.

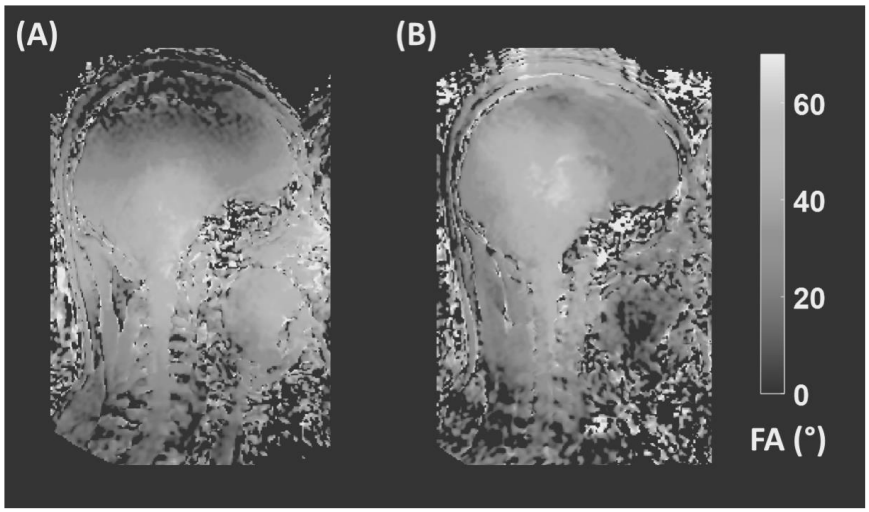
(A)
(B)
60
40
20
0
FA (°)

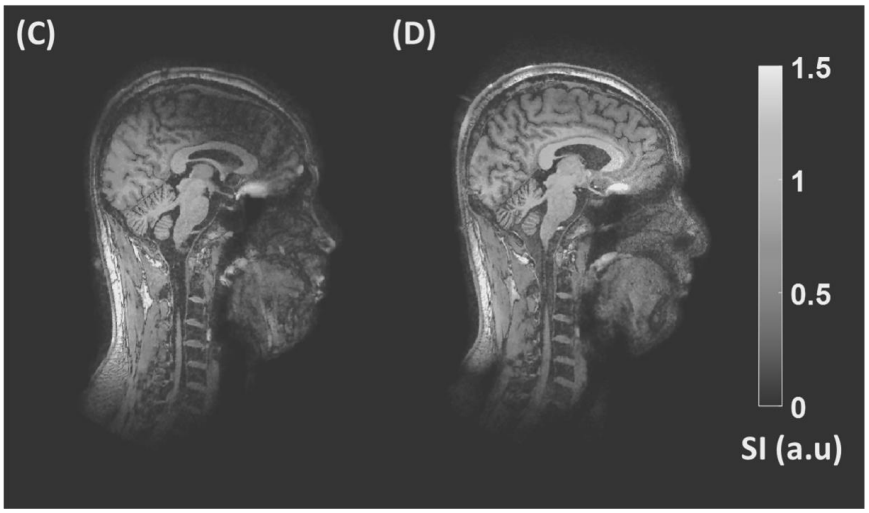
(C)
(D)
1.5
1
0.5
0
SI (a.u)

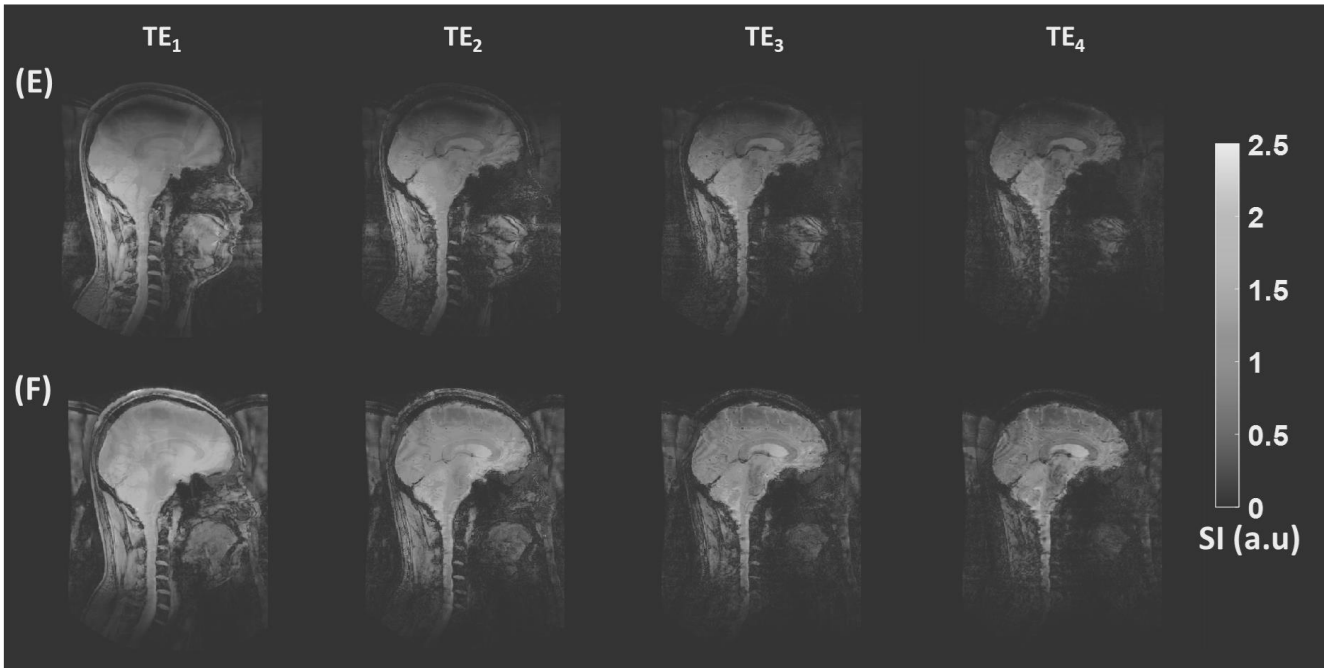
TE1
TE2
TE3
TE4
(E)
(F)
2.5
2
1.5
1
0.5
0
SI (a.u)

Table 1.

Sequence	Dual TR FA mapping	T1w - MPRAGE	T2*w - mFFE
Nominal FA (°)	60°	7°	17°
TE / TR (ms)	2 / 20,120	2.6 / 5.5 prepulse – invert (1300 ms)	3.6, 9.6, 15.6, 21.6/ 65
FOV (mm^3) RL x AP x FH	250 x 260 x 370	250 x 260 x 370	250 x 260 x 370
Acquisition matrix	320 x 320	528 x 528	768 x 768
Voxel size (mm^3)	2.5 x 2.5 x 2.5	0.7 x 0.7 x 0.7	1 x 1 x 2
SENSE factor	2 x 2	2 x 2	2 x 2
Scan time (min)	9 min 13 s	7 min 41 s	4 min 51 s

Figure Captions.

Fig. 1. Schematics and configuration of the simulated RF coil with the Duke model. **A** Birdcage only (both TX/RX), **B** Birdcage (TX) and Top-hat dipole (RX) without capacitive plate, and **C** Birdcage (TX) and Top-hat dipole (RX) with capacitive plate. The dimensions of the RF coil and capacitive plate are mentioned at the bottom.

Fig. 2. Schematic of the one-channel top-hat dipole RF coil comprising a tuning/matching circuit, balun, and active detuning pin diode, using **A** coaxial-type balun, **B** lattice LC-type balun, and constructed eight-channel top-hat dipole RF coil **C** without and **D** with capacitive plate, respectively.

Fig. 3. **A** Simulated B_1^+ field for birdcage (TX) only, birdcage (TX)/top-hat dipole (RX) without capacitive plate, and birdcage (TX)/top-hat dipole (RX) with capacitive plate and their respective **B** axial and **C** coronal slice profile indicating the improvement in B_1^+ field when using capacitive plate. **D** Simulated SI distribution for birdcage (TX/RX) only, birdcage (TX)/top-hat dipole (RX) without capacitive plate, and birdcage (TX)/top-hat dipole (RX) with capacitive plate and their respective **E** axial and **F** coronal slice.

Fig. 4. FA maps (**A, B**), high resolution T1w-MPRAGE images (**C, D**), and T2*w-mFFE images (**E, F**) of the brain using the eight-channel top-hat dipole RF coil without and with capacitive plate, respectively. Note: commercial head birdcage coil is used for the transmission.

Table Captions.

Table 1. *In vivo* MRI experiment sequence parameters.

SUPPLEMENTARY

- Single-channel electromagnetic (EM) simulations were evaluated on a uniform rectangular phantom (Height: 23.5 cm, width: 30 cm, length: 50cm) to visualize the B_1 field distribution qualitatively. The dielectric properties of the phantom include the electrical conductivity and relative permittivity of 0.68 S/m and 50.61, respectively.
- Figure below shows the dimensions of various single-channel RF coils.

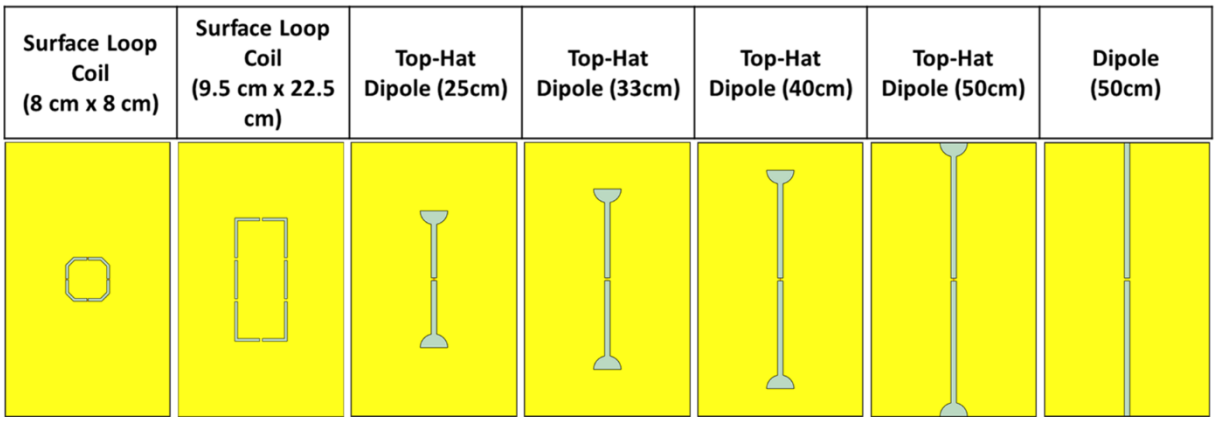

- B_1^+ field and B_1^- field were computed through the EM simulations as shown in figure A and B below. The slice profile was plotted in axial and coronal slices as shown in figure C and D, respectively.

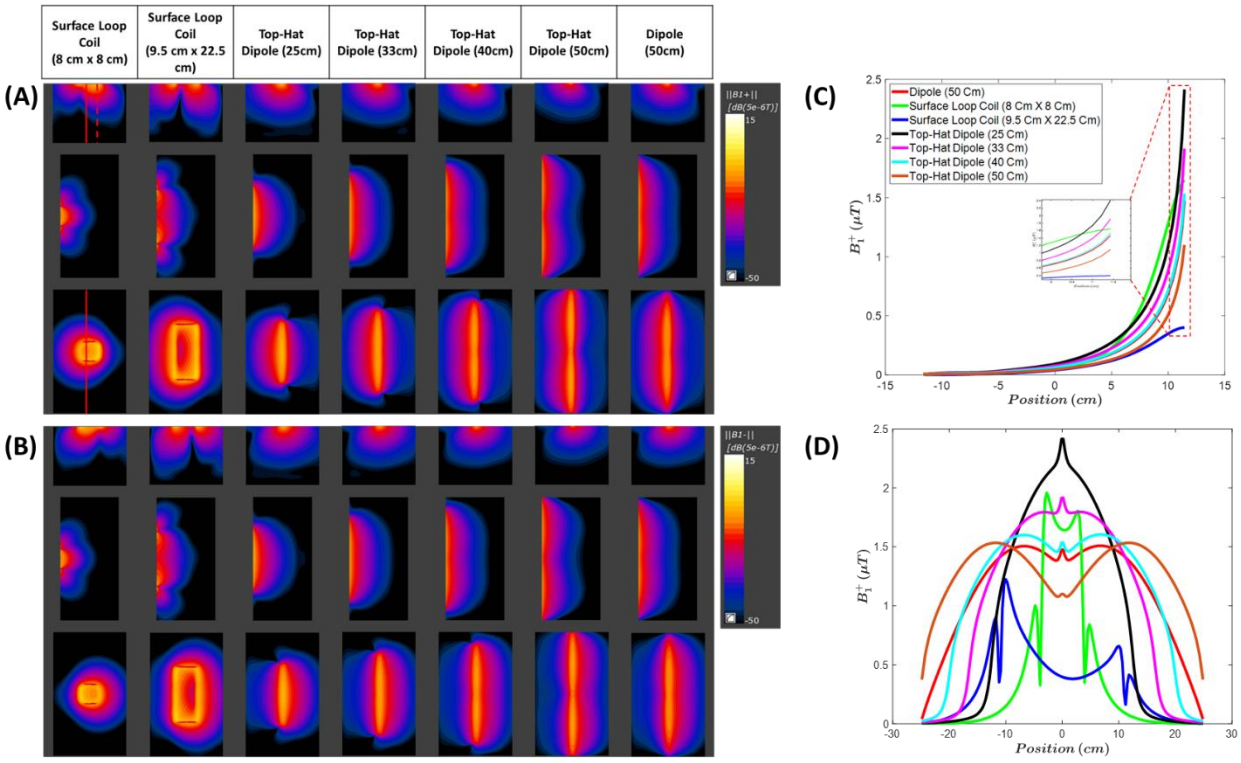

- It can be clearly seen in the simulation result that the B_1 field distribution produced by the loop RF coil is asymmetric along the center in contrast to the dipole and top-hat dipole RF coil.